Inorganic Chemistry
Article

Inorg. Chem. **2010**, *49*, 5167–5172 **5167**
DOI: 10.1021/ic100297c

The Role of Stereoactive Lone Pairs in Templated Vanadium Tellurite Charge Density Matching

Kelvin B. Chang,[†] Desmond J. Hubbard,[†] Matthias Zeller,[‡] Joshua Schrier,[†] and Alexander J. Norquist*[,†]

[†]*Department of Chemistry, Haverford College, Haverford, Pennsylvania 19041, and*
[‡]*Department of Chemistry, Youngstown State University, Youngstown, Ohio 44555*

Received February 12, 2010

The role of charge density matching was investigated in the formation of templated vanadium tellurites under mild hydrothermal conditions. Reactions were conducted using a fixed $NaVTeO_5$:amine ratio in an ethanol/water solution to isolate the effects of amine structure. The use of 1,4-diaminobutane, 1,3-diaminopropane, and piperazine resulted in three distinct vanadium tellurite connectivities, $[V_2Te_2O_{10}]_n^{2n-}$ chains, $[V_2TeO_8]_n^{2n-}$ layers, and $[V_2Te_2O_{10}]_n^{2n-}$ layers, respectively. Charge density matching with the protonated amines is the primary influence over the structure of each vanadium tellurite anion, as quantified by molecular surface area and geometric decomposition methods. Electron localization functions were calculated using the Stuttgart tight-binding linear muffin-tin orbital, atomic sphere approximation code, to visualize the location and relative size, shape, and orientation of the stereoactive lone pair in the tellurite groups. $[C_4H_{14}N_2][V_2Te_2O_{10}]$: $a = 5.649(5)$ Å, $b = 6.348(5)$ Å, $c = 9.661(5)$ Å, $\alpha = 84.860(5)°$, $\beta = 85.380(5)°$, $\gamma = 81.285(5)°$, triclinic, $P\bar{1}$ (No. 2), $Z = 1$.

Introduction

The formation of open-framework inorganic materials has been the focus of intense research since the discovery of zeolite-like aluminum phosphates in the early 1980s,[1] owing to their potential application in areas such as shape-selective catalysis, molecular sieving, and gas absorption.[2] A dramatic increase in structural diversity accompanied the incorporation of new transition and main group metals because of their ability to have coordination numbers greater than 4, a limitation of zeolites. Such materials have demonstrated a remarkable degree of compositional and structural diversity.[3,4] Sustained interest in these compounds exists because the facile formation of novel structure types and potential for tunable properties outweigh the lack of thermal stability when compared to aluminosilicate zeolites.

Selenites, iodates, and tellurites contain stereoactive lone pairs and are of interest to researchers for two reasons. First, low coordination numbers on cationic centers promote directional covalent bonding, which in turn is beneficial in the creation of new microporous materials.[3] Second, local acentricity on framework building units is a well-established route to crystallographic non-centrosymmetry.[5−10] Materials that possess crystallographic non-centrosymmetry are of great interest to researchers because they can exhibit several desirable physical properties,[11] including nonlinear optical activity, such as second harmonic generation (SHG) and piezoelectricity.[12,13] Despite the breadth of templated metal selenite chemistry and interest in metal tellurites that do not contain organic templates,[14−19] only six organically templated metal tellurites have been reported: $[C_2H_{10}N_2][VTe_3O_9]$,[20]

*To whom correspondence should be addressed. E-mail: anorquis@haverford.edu.

(1) Wilson, S. T.; Lok, B. M.; Messina, C. A.; Cannan, T. R.; Flanigen, E. M. *J. Am. Chem. Soc.* **1982**, *104*, 1146–1147.
(2) Haag, W. O. *Stud. Surf. Sci. Catal.* **1994**, *84*, 1375–1394.
(3) Cheetham, A. K.; Ferey, G.; Loiseau, T. *Angew. Chem., Int. Ed.* **1999**, *38*, 3268–3292.
(4) Rao, C. N. R.; Natarajan, S.; Neeraj, S. *J. Solid State Chem.* **2000**, *152*, 302–321.
(5) Pearson, R. G. *J. Am. Chem. Soc.* **1969**, *91*, 4947–4955.
(6) Wheeler, R. A.; Whangbo, M. H.; Hughbanks, T.; Hoffmann, R.; Burdett, J. K.; Albright, T. A. *J. Am. Chem. Soc.* **1986**, *108*, 2222–2236.
(7) Kunz, M.; Brown, I. D. *J. Solid State Chem.* **1995**, *115*, 395–406.
(8) Harrison, W. T. A.; Dussack, L. L.; Jacobson, A. J. *J. Solid State Chem.* **1996**, *125*, 234–242.
(9) Ok, K. M.; Halasyamani, P. S. *Chem. Mater.* **2002**, *14*, 2360–2364.
(10) Sykora, R. E.; Ok, K. M.; Halasyamani, P. S.; Wells, D. M.; Albrecht-Schmitt, T. E. *Chem. Mater.* **2002**, *14*, 2741–2749.
(11) Halasyamani, P. S.; Poeppelmeier, K. R. *Chem. Mater.* **1998**, *10*, 2753–2769.
(12) Kim, J.-H.; Baek, J.; Halasyamani, P. S. *Chem. Mater.* **2007**, *19*, 5637–5641.
(13) Mao, J.-G.; Jiang, H.-L.; Kong, F. *Inorg. Chem.* **2008**, *47*, 8498–8510.
(14) Harrison, W. T. A.; Buttery, J. H. N. *Z. Anorg. Allg. Chem.* **2000**, *626*, 867–870.
(15) Ok, K. M.; Halasyamani, P. S. *Chem. Mater.* **2001**, *13*, 4278–4284.
(16) Goodey, J.; Broussard, J.; Halasyamani, P. S. *Chem. Mater.* **2002**, *14*, 3174–3180.
(17) Irvine, J. T. S.; Johnston, M. G.; Harrison, W. T. A. *Dalton Trans.* **2003**, 2641–2645.
(18) Ok, K. M.; Halasyamani, P. S. *Inorg. Chem.* **2004**, *43*, 4248–4253.
(19) Johnston, M. G.; Harrison, W. T. A. *Acta Crystallogr. Sect. C* **2007**, *C63*, i57–i59.
(20) Gao, B.; Liu, S.; Xie, L.; Wang, X.; Zhang, C.; Sun, C.; Hu, N.; Jia, H. *J. Solid State Chem.* **2005**, *178*, 1825–1829.

Published on Web 05/11/2010

$[C_2H_{10}N_2][V_2Te_2O_{10}]\cdot H_2O$,[21] $[C_4H_{12}N_2][(VO_2)(TeO)_3]_2$,[21] $[C_3H_{12}N_2][V_2TeO_8]$,[22] $[C_4H_{15}N_3][V_2Te_2O_{10}]\cdot 2H_2O$,[23] and $[C_2H_{10}N_2][VTeO_5]_2$.[24]

A number of reaction mechanisms have been postulated for the formation of organically templated inorganic materials.[25−28] Ferey proposed that charge density matching between the positively charged amine and negatively charged secondary building unit (SBU) results in neutral ammonium−SBU pairs and provides the thermodynamic driving force and structural organization during precipitation.[25,26] The charge densities of the amines are generally fixed by pH, while structural modulations in the inorganic components allow for the formation of neutral pairs. In this paper, the role of charge density matching in organically templated vanadium tellurites is studied in the context of one new compound, $[C_4H_{14}N_2][V_2Te_2O_{10}]$, and two recently reported compounds, $[C_3H_{12}N_2][V_2TeO_8]$[22] and $[C_4H_{12}N_2][(VO_2)(TeO_3)]_2$.[21] The effects of the tellurite stereoactive lone pairs are probed through the use of electron localization functions (ELFs).

Experimental Section

Materials. Na_2CO_3 (99.5%), V_2O_5 (98%), TeO_2 (99%), 1,3-diaminopropane (1,3-dap, 99%), 1,4-diaminobutane (1,4-dab, 99%), glacial acetic acid, and piperazine (pip, 99%) were purchased from Aldrich and used as received. Ethanol was purchased from Pharmaco. Deionized water was used in these syntheses.

Synthesis. All reactions were conducted in 15 mL polypropylene screw top bottles. Compound **1**, $[C_3H_{12}N_2][V_2TeO_8]$,[22] and $[C_4H_{12}N_2][(VO_2)(TeO_3)]_2$[21] were synthesized from mixtures of $NaVTeO_5$[29,30] and an amine in an ethanol/water solution. Glacial acetic acid was used to adjust the pH of each reaction gel to a value of approximately 5. Reactions were heated to 100 °C and allowed to soak for 86 h. Bottles were opened in air, and products were recovered through filtration. The postreaction solution pH for each reaction was between 4 and 5. Reaction yields ranged between 90% and 95%, based upon tellurium.

$[C_4H_{14}N_2][V_2Te_2O_{10}]$ (1) was synthesized through the reaction of 0.2843 g (1.010×10^{-4} mol) of $NaVTeO_5$, 0.7093 g (8.060×10^{-3} mol) of 1,4-dab, 2.5 mL of ethanol, and 2.5 mL of deionized water. Colorless needles were produced. IR data: N−H 1462, 1482, 1607 cm^{-1}, C−H 3121 cm^{-1}, Te−O 738 cm^{-1}, Te−O−Te 493, 648 cm^{-1}, V = O 825 cm^{-1}.

Single-Crystal X-ray Diffraction. Data were collected using a Bruker AXS Smart Apex CCD diffractometer with Mo Kα radiation (λ = 0.71073 Å). A single crystal was mounted on a Mitegen micromesh mount using a trace of mineral oil and cooled *in situ* to 100(2) K for data collection. Frames were collected, indexed, and processed and the files scaled and corrected for absorption using APEX2.[31] The heavy atom positions were determined using SIR92.[32] All other non-hydrogen sites were located from Fourier difference maps. All non-hydrogen sites were refined using anisotropic thermal parameters using full matrix least-squares procedures on F_o^2 with $I > 3\sigma(I)$. Hydrogen atoms were placed in geometrically idealized positions. All calculations were performed using Crystals.[33] Relevant crystallographic data are listed in Table 1.

Table 1. Crystallographic Data for $[C_4H_{14}N_2][V_2Te_2O_{10}]$ (**1**)

compound	$[C_4H_{14}N_2][V_2Te_2O_{10}]$
formula	$C_4H_{14}N_2O_{10}Te_2V_2$
fw	607.24
space group	$P\bar{1}$ (No. 2)
a/Å	5.649(5)
b/Å	6.348(5)
c/Å	9.661(5)
α/deg	84.860(5)
β/deg	85.380(5)
γ/deg	81.284(5)
V/Å^3	340.3(4)
Z	1
ρ_{calc}/g cm^{-3}	2.963
λ/Å	0.71073
T/K	100(2)
μ/mm^{-1}	5.625
R_1[a]	0.0214
wR_2[b]	0.0475

[a] $R_1 = \sum\|F_o| - |F_c\|/\sum|F_o|$. [b] $wR_2 = [\sum w(F_o^2 - F_c^2)^2/[\sum w(F_o^2)^2]]^{1/2}$.

Powder X-ray Diffraction. Powder diffraction patterns were recorded on a GBC-Difftech MMA powder diffractometer. Samples were mounted on aluminum plates. Calculated powder patterns were generated from single-crystal data using ATOMS *v*. 6.0.[34] Powder X-ray diffraction was used to support the structure determination of **1** and confirm the syntheses of $[C_3H_{12}N_2][V_2TeO_8]$ and $[C_4H_{12}N_2][(VO_2)(TeO_3)]_2$. Experimental powder X-ray diffraction patterns matched simulated patterns.

Infrared Spectroscopy. Infrared measurements were obtained using a Perkin-Elmer FT-IR Spectrum 1000 spectrophotometer. A sample was diluted with spectroscopic grade KBr and pressed into a pellet. The scan was run over the range 400−4000 cm^{-1}.

Surface Area Calculations. Surface areas for the inorganic components in $[C_4H_{14}N_2][V_2Te_2O_{10}]$ (**1**), $[C_3H_{12}N_2][V_2TeO_8]$, and $[C_4H_{12}N_2][(VO_2)(TeO_3)]_2$ were calculated using the DMS program,[35] defined by Richards[36] as the molecular surface, and a geometric decomposition method[37] that involves reducing complex surface structures into polygons. A probe radius of 1.5 Å was used in molecular surface area calculations, and van der Waals radii of 1.52 and 2.00 Å were used for oxygen and metal atoms, respectively. Lone pair radii were set to 1.5 Å, based upon Galy's determination of lone pair volumes in vanadium tellurites.[38,39] Lone pair positions were determined using ELF isosurfaces, as described below. Calculated surface areas are listed in Table 2. Values are reported for a single anion formula unit. Linear fits were used to remove edge effects from the truncated 2D structures when using DMS.

Electron Localization Functions. Solid-state electronic structure calculations were performed using version 47 of the Stuttgart

(21) Feng, M.-L.; Mao, J.-G. *J. Solid State Chem.* **2005**, *178*, 2256–2261.
(22) Huang, X.; Liu, Z.; Huang, C.; Shen, L.; Yan, X. *Acta Crystallogr. Sect. C* **2009**, *C65*, m404–m406.
(23) Huang, X.; Liu, Z.; Huang, C.; Shen, L.; Yan, X. *Acta Crystallogr. Sect. C* **2009**, *C65*, m385–m387.
(24) Jung, K.; Kim, H.; Yun, H.; Do, J. *Z. Anorg. Allg. Chem.* **2006**, *632*, 1582–1585.
(25) Ferey, G. *J. Fluorine Chem.* **1995**, *72*, 187–193.
(26) Ferey, G. *Chem. Mater.* **2001**, *13*, 3084–3098.
(27) Rao, C. N. R.; Natarajan, S.; Choudhury, A.; Neeraj, S.; Ayi, A. A. *Acc. Chem. Res.* **2001**, *34*, 80–87.
(28) Murugavel, R.; Walawalkar, M. G.; Dan, M.; Roesky, H. W.; Rao, C. N. R. *Acc. Chem. Res.* **2004**, *37*, 763–774.
(29) Rozier, P.; Vendier, L.; Galy, J. *Acta Crystallogr. Sect. C* **2002**, *C58*, i111–i113.
(30) Darriet, J.; Guillaume, G.; Wilhelmi, K. A.; Galy, J. *Acta Chem. Scand.* **1972**, *26*, 59–70.
(31) *Apex2 v2009.7-0*. Bruker AXS Inc.: Madison, WI, 2009.
(32) Altomare, A.; Cascarano, G.; Giacovazzo, C.; Guagliardi, A. *J. Appl. Crystallogr.* **1993**, *26*, 343–350.
(33) Betteridge, P. W.; Carruthers, J. R.; Cooper, R. I.; Prout, K.; Watkin, D. J. *J. Appl. Crystallogr.* **2003**, *36*, 1487.
(34) Dowty, E. *ATOMS v. 6.0*; Shape Software: Kingsport, TN, 2002.
(35) Huang, C. *DMS*; Computer Graphics Lab, University of California: San Francisco, CA, 2002.
(36) Richards, F. M. *Annu. Rev. Biophys. Bioeng.* **1977**, *6*, 151–176.
(37) Casalongue, H. S.; Choyke, S. J.; Narducci Sarjeant, A.; Schrier, J.; Norquist, A. J. *J. Solid State Chem.* **2009**, *182*, 1297–1303.
(38) Andersson, S.; Astrom, A.; Galy, J.; Meunier, G. *J. Solid State Chem.* **1973**, *6*, 187–190.
(39) Galy, J.; Meunier, G.; Andersson, S.; Astrom, A. *J. Solid State Chem.* **1975**, *13*, 142–159.

Table 2. Surface Area and Charge Density Results for $[C_4H_{14}N_2][V_2Te_2O_{10}]$ (**1**), $[C_3H_{12}N_2][V_2TeO_8]$,[22] and $[C_4H_{12}N_2][(VO_2)(TeO_3)]_2$[21]

compound	anion	method		surface area (Å^2)	anion charge	charge density (e Å^{-2})
$[C_4H_{14}N_2][V_2Te_2O_{10}]$	$[V_2Te_2O_{10}]_n^{2n-}$ chains	geometric decomposition	model 1	93.4	−1.96	−0.0210
			model 2	95.7		−0.0205
		molecular surface		98.9		−0.0198
$[C_3H_{12}N_2][V_2TeO_8]$	$[V_2TeO_8]_n^{2n-}$ layers	geometric decomposition		97.6	−1.68	−0.0214
		molecular surface		90.4		−0.0186
$[C_4H_{12}N_2][(VO_2)(TeO_3)]_2$	$[V_2Te_2O_{10}]_n^{2n-}$ layers	geometric decomposition		76.4	−1.88	−0.0246
		molecular surface		79.8		−0.0236

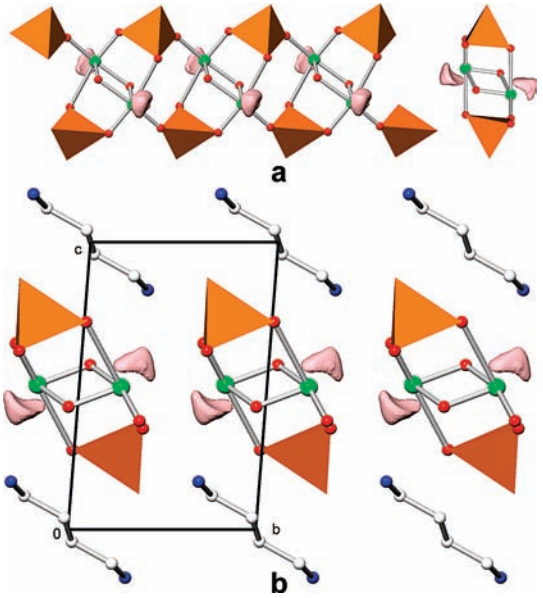

Figure 1. (a) $[V_2Te_2O_{10}]_n^{2n-}$ chains and (b) three-dimensional packing in $[C_4H_{14}N_2][V_2Te_2O_{10}]$. ELF isosurfaces are shown with a boundary condition of 0.78. Green and red spheres represent tellurium and oxygen atoms, respectively, while orange polyhedra represent $[VO_4]$.

tight-binding linear muffin-tin orbital, atomic sphere approximation (TB-LMTO-ASA) code,[40,41] utilizing the experimental crystal structures. This method replaces the core electrons with a pseudopotential. It is known that the valence-electron-density ELF quantitatively differs from all-electron values, but does not alter the qualitative results except for the lack of core basins.[42] Consequently, the discussion of ELF isosurfaces will be restricted to qualitative properties. The isolated vacuum-phase molecular cation ELF isosurfaces were calculated at the B3LYP/6-31G*//B3LYP/6-311+G(d,p) level using Gaussian03[43] and the TopMod package.[44]

Results

$[C_4H_{14}N_2][V_2Te_2O_{10}]$ (**1**) contains a single four-coordinate vanadium center, in which the $V-O_{terminal}$ distance is 1.635(2) Å, while $V-O_{bridging}$ bonds are generally longer, at 1.659(2) to 1.849(2) Å. The coordination environment of the single unique Te^{4+} center in $[C_4H_{14}N_2][V_2Te_2O_{10}]$ is a distorted square pyramid, two of which share two oxides to form $[Te_2O_8]$ dimers. Two distinct Te−O bonds are observed in which the oxygen bridges between two Te^{4+} centers, with distances of 1.883(2) and 2.168(2) Å. Three Te−O bonds are observed in which the oxygen bridges between a V^{5+} and a Te^{4+} center, with distances ranging between 1.883(2) and 2.694(2) Å.

Connection of the $[Te_2O_8]$ dimers and $[VO_4]$ tetrahedra results in $[V_2Te_2O_{10}]_n^{2n-}$ chains. The stereoactive lone pairs on each Te^{4+} center are aligned in a perpendicular fashion with respect to the direction of chain propagation and in an antiparallel fashion with respect to one another within each dimer. An extensive three-dimensional hydrogen-bonding network exists between the $[V_2Te_2O_{10}]_n^{2n-}$ chains and $[C_4H_{14}N_2]^{2+}$ cations. The chain connectivity and three-dimensional packing of $[C_4H_{14}N_2][V_2Te_2O_{10}]$ are shown in Figure 1.

Bonding Networks. The bonding network present in $[C_4H_{14}N_2][V_2Te_2O_{10}]$ was analyzed using bond valence sums;[45,46] see Table 3. The calculated $\sum S_i$ values for each cation correspond to their oxidation states. The second-order Jahn−Teller (SOJT)[5−7] distortions in the Te^{4+} cations are manifested in their asymmetric coordination environments. While V^{5+} cations have the correct electronic configuration to exhibit SOJT distortions, they lack the required octahedral coordination geometries.

Electron Localization Function Plots. The electron localization function[47,48] isosurface has been used previously to characterize lone pairs in solids.[49−54] Strictly

(40) Andersen, O. K. *Phys. Rev. B* **1975**, *12*, 3060–3083.
(41) Andersen, O. K.; Jepsen, O. *Phys. Rev. Lett.* **1984**, *53*, 2571–2574.
(42) Kohout, M.; Savin, A. *J. Comput. Chem.* **1997**, *18*, 1431–1439.
(43) Frisch, M. J.; Trucks, G. W.; Schlegel, H. B.; Scuseria, G. E.; Robb, M. A.; Cheeseman, J. R.; Montgomery, J. A., Jr.; Vreven, T.; Kudin, K. N.; Burant, J. C.; Millam, J. M.; Iyengar, S. S.; Tomasi, J.; Barone, V.; Mennucci, B.; Cossi, M.; Scalmani, G.; Rega, N.; Petersson, G. A.; Nakatsuji, H.; Hada, M.; Ehara, M.; Toyota, K.; Fukuda, R.; Hasegawa, J.; Ishida, M.; Nakajima, T.; Honda, Y.; Kitao, O.; Nakai, H.; Klene, M.; Li, X.; Knox, J. E.; Hratchian, H. P.; Cross, J. B.; Bakken, V.; Adamo, C.; Jaramillo, J.; Gomperts, R.; Stratmann, R. E.; Yazyev, O.; Austin, A. J.; Cammi, R.; Pomelli, C.; Ochterski, J. W.; Ayala, P. Y.; Morokuma, K.; Voth, G. A.; Salvador, P.; Dannenberg, J. J.; Zakrzewski, V. G.; Dapprich, S.; Daniels, A. D.; Strain, M. C.; Farkas, O.; Malick, D. K.; Rabuck, A. D.; Raghavachari, K.; Foresman, J. B.; Ortiz, J. V.; Cui, Q.; Baboul, A. G.; Clifford, S.; Cioslowski, J.; Stefanov, B. B.; Liu, G.; Liashenko, A.; Piskorz, P.; Komaromi, I.; Martin, R. L.; Fox, D. J.; Keith, T.; Al-Laham, M. A.; Peng, C. Y.; Nanayakkara, A.; Challacombe, M.; Gill, P. M. W.; Johnson, B.; Chen, W.; Wong, M. W.; Gonzalez, C.; Pople, J. A. *Gaussian 03, Revision E.01*; Gaussian, Inc.: Wallingford, CT, 2004.
(44) Noury, S.; Krokidis, X.; Fuster, F.; Silvi, B. *TopMoD Package*; Universite Pierre et Marie Curie, 1997.
(45) Brown, I. D.; Altermatt, D. *Acta Crystallogr. Sect. B* **1985**, *41*, 244–247.
(46) Brese, N. E.; O'Keeffe, M. *Acta Crystallogr. Sect. B* **1991**, *47*, 192–197.
(47) Becke, A. D.; Edgecombe, K. E. *J. Chem. Phys.* **1990**, *92*, 5397–5403.
(48) Silvi, B.; Savin, A. *Nature* **1994**, *371*, 683–686.

Table 3. Bond Valence Sums for $[C_4H_{14}N_2][V_2Te_2O_{10}]$ (**1**)

S_i	V1	Te1	$\sum S_i$	$V - \sum S_i$
O1		0.60	1.89	−0.11
		1.29		
O2	0.88	1.07	1.95	−0.05
O3	1.05	0.94	1.99	−0.01
O4	1.48	0.14	1.62	−0.38
O5	1.57		1.57	−0.43
ΣS_i	4.98	4.04		

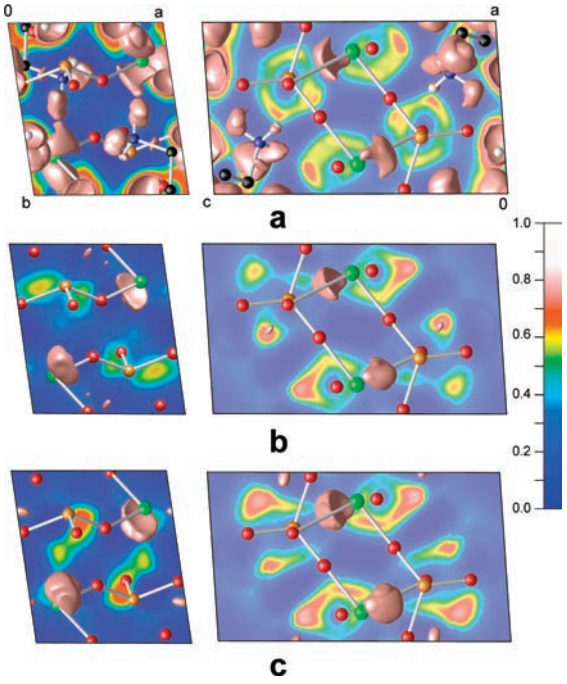

Figure 2. ELF isosurface plots of (a) $[C_4H_{14}N_2][V_2Te_2O_{10}]$, (b) isolated $[V_2Te_2O_{10}]$ chains, and (c) isolated $[V_2Te_2O_{10}]$ chains with shifted empty spheres. Green, orange, red, blue, gray, and white spheres represent tellurium, vanadium, oxygen, nitrogen, carbon, and hydrogen atoms, respectively. ELF isosurfaces are shown with a boundary condition of 0.78.

speaking, the ELF is determined by the charge density and its nodal characteristics, rather than electron pairing *per se*,[55] but nonetheless corresponds to chemical intuitions of localized bonds and lone pairs.[48]

ELF isosurfaces were calculated for $[C_4H_{14}N_2][V_2Te_2O_{10}]$ (**1**), $[C_3H_{12}N_2][V_2TeO_8]$,[22] and $[C_4H_{12}N_2][(VO_2)(TeO_3)]_2$.[21] The ELF isosurface for **1** is shown in Figure 2a. Lobelike, monosynaptic ELF basins are observed near each Te^{4+} cation, consistent with stereoactive lone pairs. Additional isosurfaces are observed in the organic amines in **1**, which have highly localized electrons[56] that complicate these figures. An ELF isosurface plot for $[C_4H_{14}N_2]^{2+}$ is provided in the Supporting Information. No qualitative differences exist between the ELF isosurfaces of the isolated $[C_4H_{14}N_2]^{2+}$ cations and the cations in the crystal, suggesting that the organic cations play a structural role in the material, but do not modify the lone pair on the Te^{4+} atoms.

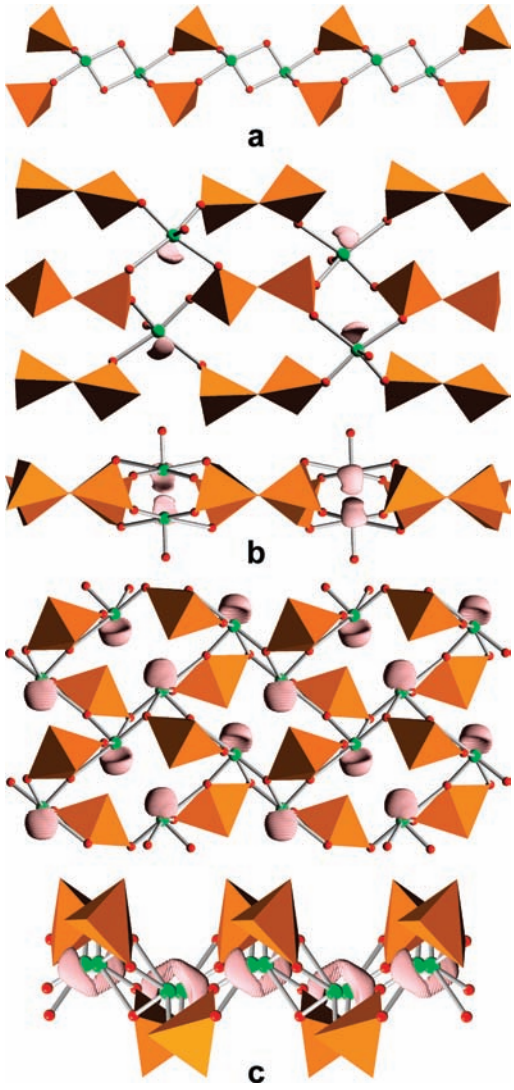

Figure 3. (a) $[V_2Te_2O_{10}]_n^{2n-}$ chains in $NaVTeO_5$ and ELF isosurface plots of isolated vanadium tellurite layers in (b) $[C_3H_{12}N_2][V_2TeO_8]$ and (c) $[C_4H_{12}N_2][(VO_2)(TeO_3)]_2$. Green and red spheres represent tellurium and oxygen atoms, respectively, while orange polyhedra represent either $[VO_4]$ or $[VO_5]$. ELF isosurfaces are shown with a boundary condition of 0.78.

To focus more clearly on the anion, additional TB-LMTO-ASA calculations were performed on **1** after removal of the organic amines from the model. The resulting ELF isosurface is shown in Figure 2b. Although these calculations were performed on neutral species rather than anions, a visual comparison of isosurfaces in Figure 2a,b shows that the ELF isosurfaces in the inorganic regions are qualitatively unchanged in location, size, shape, and orientation. Both calculations result in highly localized electron density where one would expect Te^{4+} lone pairs. Figures of the isolated vanadium tellurite anions in **1**, $[C_3H_{12}N_2][V_2TeO_8]$, and $[C_4H_{12}N_2][(VO_2)(TeO_3)]_2$

(49) Seshadri, R.; Hill, N. A. *Chem. Mater.* **2001**, *13*, 2892–2899.
(50) Stoltzfus, M. W.; Woodward, P. M.; Seshadri, R.; Klepeis, J.-H.; Bursten, B. *Inorg. Chem.* **2007**, *46*, 3839–3850.
(51) Waghmare, U. V.; Spaldin, N. A.; Kandpal, H. C.; Seshadri, R. *Phys. Rev. B* **2003**, *67*, 125111.
(52) Raulot, J.-M.; Baldinozzi, G.; Seshadri, R.; Cortona, P. *Solid State Sci.* **2002**, *4*, 467–474.
(53) Rodriguez, E. E.; Poineau, F.; Llobet, A.; Czerwinski, K.; Seshadri, R.; Cheetham, A. K. *Inorg. Chem.* **2008**, *47*, 6281–6288.
(54) Chang, H.-Y.; Kim, S.-H.; Halasyamani, P. S.; Ok, K. M. *J. Am. Chem. Soc.* **2009**, *131*, 2426–2427.
(55) Burdett, J. K.; McCormick, T. A. *J. Phys. Chem. A* **1998**, *102*, 6366–6372.
(56) Chesnut, D. B. *J. Phys. Chem. A* **2000**, *104*, 7635–7638.

that include lone pair isosurfaces are shown in Figures 1 and 3.

Small isolated ELF isosurfaces, which are not centered around atoms, are observed in the calculations on **1**, as shown in Figure 2b. Essentially all solid-state structures require the inclusion of interstitial empty spheres in TB-LMTO-ASA calculations to provide a description of the electron density throughout the unit cell. The empty spheres included in these calculations only serve to complete the basis and can be chosen arbitrarily. However, these spheres still do not fill all of the spaces, leading to artificially abrupt changes in the charge density at the boundaries of these spheres. We speculate that this is the cause of the small isolated ELF regions. To probe the effects of these empty spheres, half of the original spheres were removed, and the radii of the remaining spheres were reduced. This was followed by the introduction of additional empty spheres to fill the unit cell. A plot of the ELF isosurface in compound **1** after the empty sphere shifts is shown in Figure 2c. The results were pronounced shifts in the sizes, shapes, and positions of these small isolated ELF isosurfaces, but not the larger atom-centered isosurfaces. Therefore, we conclude that the former are artifacts of the arbitrary and somewhat incomplete basis choice in the TB-LMTO-ASA procedure rather than being physically meaningful. In addition, the essentially unchanged inorganic isosurface features result from the nature of the electron interactions in the (unchanged) potential of the inorganic structures.

Discussion

This study was designed to better elucidate formation mechanisms by isolating the effects of amine structure. Compound **1**, $[C_3H_{12}N_2][V_2TeO_8]$,[22] and $[C_4H_{12}N_2][(VO_2)(TeO_3)]_2$[21] were all synthesized under nearly identical reaction conditions using $NaVTeO_5$ as a source of both V^{5+} and Te^{4+}. These three compounds were synthesized from reaction gels with fixed 1 $NaVTeO_5$:8 amine ratio in a 1:1 ethanol/H_2O solution. The only difference between reactions was the identity of the amine.

$NaVTeO_5$[30] was selected as a source for both V^{5+} and Te^{4+} for two reasons. First, the solubility of $NaVTeO_5$ is substantially greater than V_2O_5 and TeO_2 under the conditions employed in this study. This provides access to more gentle reaction conditions, which have been shown to promote the formation of lower density, more open structures.[57] In addition, reactions at higher temperature tend to promote the reduction of Te^{4+} to tellurium metal under the conditions described above. Specifically, we observed the formation of elemental tellurium in reactions conducted at 180 °C or above using TeO_2. Second, $NaVTeO_5$ contains both V^{5+} and Te^{4+} in a single compound, enabling the simplification of the reaction conditions. The presence of Na^+ cations in $NaVTeO_5$ is not expected to greatly influence the nature of the reaction products. While the Na^+ affects the ionic strength of the solution, it remains in solution after reaction and is not incorporated into the crystalline products.

The role of amines in the formation of new inorganic materials is well known.[25,26] Charge density matching between the amine and inorganic component is thought to govern the formation of neutral ammonium−secondary building unit pairs, from which oligomerization and precipitation can occur. The determination of the inorganic topology is therefore dependent upon the size, shape, and charge of the protonated organic amines. The effects of charge density matching have been demonstrated in several systems using different methods, with notable examples including lamellar and hexagonal silicate[58−60] and oxovanadium phosphate[61] mesostructures. However, the determination of accurate charge densities of complex inorganic architectures requires the availability of surface area data. While various techniques for calculating surface areas have been reported recently,[62−64] two complementary methods are employed in this study. As shown in Table 2, these give the same qualitative results.

An inherent assumption in the determination of the molecular surface, as described by Richards,[36] is that the use of a spherical probe is appropriate. A probe radius of 1.5 Å was used to reflect the van der Waals radius of N.[65] The sum of the probe radius and the van der Waals radius of O approximates the outer limit of most hydrogen-bonding interactions of ∼3.0 Å. As the probe radius is based upon the length of hydrogen bonds, the molecular surfaces calculated with DMS should represent the maximum possible surface area for a specific anionic structure.

Steric effects associated with other parts of a generally nonspherical organic amine probe can reduce the accessible surface area. Our geometrical decomposition method allows for the exclusion of the small openings between secondary building units in structures shown in Figures 1 and 3. The differences between the surface areas calculated using the geometric decomposition method and the molecular surface determined using the DMS program provide a suitable range of surface areas that reflect both the length of the N−H···O interactions and the nonspherical nature of the organic amines used in this study.

The inclusion of stereoactive lone pairs in surface area calculations requires both their positions and volumes. Local maxima in the electron localization functions were set as the centers of the lone pairs, which were approximated as spheres with radii of 1.5 Å, consistent with Galy's work on lone pair volumes in such systems.[38,39] Geometric decomposition models for the vanadium tellurite anions in **1**, $[C_3H_{12}N_2][V_2TeO_8]$, and $[C_4H_{12}N_2][(VO_2)(TeO_3)]_2$ are shown in the Supporting Information.

The inorganic structures described in this study are all anionic. Bond valence sums were used to quantify the residual charges[66−68] on each atom site. In general, charges

(57) Forster, P. M.; Burbank, A. R.; Livage, C.; Ferey, G.; Cheetham, A. K. *Chem. Commun.* **2004**, 368–369.

(58) Tolbert, S. H.; Landry, C. C.; Stucky, G. D.; Chmelka, B. F.; Norby, P.; Hanson, J. C.; Monnier, A. *Chem. Mater.* **2001**, *13*, 2247–2256.

(59) Huo, Q.; Margolese, D. I.; Ciesla, U.; Feng, P.; Gier, T. E.; Sieger, P.; Leon, R.; Petroff, P. M.; Schueth, F.; Stucky, G. D. *Nature* **1994**, *368*, 317–321.

(60) Monnier, A.; Schuth, F.; Huo, Q.; Kumar, D.; Margolese, D.; Maxwell, R. S.; Stucky, G. D.; Krishnamurty, M.; Petroff, P.; Firouzi, A.; Janicke, M.; Chmelka, B. F. *Science* **1993**, *261*, 1299–1303.

(61) El Haskouri, J.; Roca, M.; Cabrera, S.; Alamo, J.; Beltran-Porter, A.; Beltran-Porter, D.; Marcos, M. D.; Amoros, P. *Chem. Mater.* **1999**, *11*, 1446–1454.

(62) Maggard, P. A.; Boyle, P. D. *Inorg. Chem.* **2003**, *42*, 4250–4252.

(63) Krivovichev, S. V.; Tananaev, I. G.; Myasoedov, B. F. *C. R. Chim.* **2007**, *10*, 897–904.

(64) Ling, J.; Sigmon, G. E.; Burns, P. C. *J. Solid State Chem.* **2009**, *182*, 402–408.

(65) Bondi, A. *J. Phys. Chem.* **1964**, *68*, 441–451.

(66) Welk, M. E.; Norquist, A. J.; Stern, C. L.; Poeppelmeier, K. R. *Inorg. Chem.* **2000**, *39*, 3946–3947.

are largely localized on oxide anions with metal sites retaining little residual charge, as shown in Table 3 and the Supporting Information. Only atom sites on the surface of each layer contribute to the charge felt by the organic amine cations. The charges on atoms that reside in the interior of a given layer are shielded from the amines by neighboring V^{5+} and Te^{4+} cations.

As noted by Ferey, the charge density of an amine is largely dependent upon its acidity.[25] The linear diamines 1,3-dap and 1,4-dab have significantly higher pK_1 values with respect to the more spherical piperazine, resulting in lower charge densities. This trend is reflected in the decreased charge densities of the vanadium tellurite anions in **1** and $[C_3H_{12}N_2][V_2TeO_8]$ with respect to $[C_4H_{12}N_2][(VO_2)(TeO_3)]_2$. The calculated charge density ranges of the inorganic components in **1** and $[C_3H_{12}N_2][V_2TeO_8]$ are -0.0198 to -0.0210 and -0.0186 to -0.0214 e Å^{-2}, respectively. In contrast, the charge density of the $[V_2Te_2O_{10}]_n^{2n-}$ layers in $[C_4H_{12}N_2][(VO_2)(TeO_3)]_2$ is significantly higher, with values ranging between -0.0236 and -0.0246 e Å^{-2}. This reflects the increase charge density of the $[pipH_2]^{2+}$ cations with respect to $[1,3\text{-}dapH_2]^{2+}$ or $[1,4\text{-}dabH_2]^{2+}$.

While the composition of the inorganic components is unchanged between **1** and $[C_4H_{12}N_2][(VO_2)(TeO_3)]_2$, their connectivities and charge densities differ greatly. The $[V_2Te_2O_{10}]_n^{2n-}$ chains in **1** and layers in $[C_4H_{12}N_2][(VO_2)(TeO_3)]_2$ are both constructed from tellurite dimers and vanadium monomers. However, the ways in which these primary building units assemble to form secondary building units reflect the differences in charge densities of the respective amines, resulting in different structures. While many influences are present in the determination of the inorganic structure,[37] charge density matching appears to exert the greatest impact on the inorganic topology.

Acknowledgment. The authors thank Ram Seshadri for helpful suggestions on the calculations of ELFs and acknowledge support from the NSF (Award No. CHE-0911121) and grants to Haverford College from the HHMI Undergraduate Science Education Program. M.Z. acknowledges support for the purchase of a diffractometer from the NSF grant 0087210, the Ohio Board of Regents grant CAP-491, and Youngstown State University.

Supporting Information Available: Bond valence sum analyses of $[C_3H_{12}N_2][V_2TeO_8]$ and $[C_4H_{12}N_2][(VO_2)(TeO_3)]_2$, an ELF isosurface plot of $[C_4H_{14}N_2]^{2+}$, perspective views of the ELF isosurfaces of the inorganic components in $[C_4H_{14}N_2][V_2Te_2O_{10}]$, $[C_3H_{12}N_2][V_2TeO_8]$, and $[C_4H_{12}N_2][(VO_2)(TeO_3)]_2$, and views of the geometric decomposition models for $[C_4H_{14}N_2][V_2Te_2O_{10}]$ (**1**), $[C_3H_{12}N_2][V_2TeO_8]$, and $[C_4H_{12}N_2][(VO_2)(TeO_3)]_2$. An X-ray crystallographic information file (CIF) is available for $[C_4H_{14}N_2][V_2Te_2O_{10}]$. This material is available free of charge via the Internet at http://pubs.acs.org.

(67) Norquist, A. J.; Doran, M. B.; O'Hare, D. *Inorg. Chem.* **2005**, *44*, 3837–3843.
(68) Veltman, T. R.; Stover, A. K.; Sarjeant, A. N.; Ok, K. M.; Halasyamani, P. S.; Norquist, A. J. *Inorg. Chem.* **2006**, *45*, 5529–5537.